DR. YUXI PANG (Orcid ID : 0000-0001-5039-0236)

Article type : Full Paper

An order parameter without magic angle effect (OPTIMA) derived from $R_{1\rho}$ dispersion in ordered tissue

Yuxi Pang, PhD

Department of Radiology, University of Michigan, Ann Arbor, MI, USA

Corresponding Author:

Yuxi Pang, PhD
University of Michigan Hospital
1500 E. Medical Center Dr., UH B2 RM A205F
Ann Arbor, MI 48109-5030, USA
Tel: 734-232-6585
Fax: 734-764-2412

This is the author manuscript accepted for publication and has undergone full peer review but has not been through the copyediting, typesetting, pagination and proofreading process, which may lead to differences between this version and the Version of Record. Please cite this article as doi: 10.1002/MRM.28045

Email: yuxipang@umich.edu
Twitter: @yuxipang
ORCID iD: Yuxi Pang (https://orcid.org/0000-0001-5039-0236)

Running Title: An orientation-independent MR metric derived from $R_{1\rho}$ dispersion in ordered tissue

Word Count: 5,249

ABSTRACT

Purpose: Magnetic resonance R_2 imaging of ordered tissue exhibits the magic angle effect, potentially masking subtle pathological changes in cartilage. This work aimed to develop an orientation-independent order parameter (S) exclusively sensitive to collagen degeneration.

Methods: A theory was developed based on $R_{1\rho}$ dispersion coupled with a simplified molecular motion model, where anisotropic $R_2^q(\theta)$ became directly proportional to correlation time $\tau_b(\theta)$ and S could be derived. This new parameter was validated with ex vivo $R_{1\rho}$ dispersion reported on orientated (n=4), enzymatically depleted bovine cartilage (n=6) and osteoarthritic human knee specimens (n=14) at 9.4T, and further demonstrated on one healthy human knee in vivo at 3T.

Results: $\tau_b(\theta)$ from orientation-dependent $R_{1\rho}$ dispersion revealed a significantly high average correlation ($r = 0.89 \pm 0.05$, $P < 0.05$) with $R_2^q(\theta)$ on cartilage samples and a moderate correlation ($r = 0.48$, $P < 0.001$) for the human knee in vivo. The derived S (10^{-3}) significantly decreased in advanced osteoarthritis (1.64±0.03 vs. 2.30±0.11, $P < 0.001$) and collagen-depleted samples (1.30±0.11 vs. 2.12±0.12, $P < 0.001$) when compared with early osteoarthritis and the control, respectively.

Conclusion: The proposed order parameter could be a potentially useful orientation-independent MR biomarker for collagen alterations in cartilage and other highly structured tissues.

Key words: order parameter, $R_{1\rho}$ dispersion, magic angle effect, anisotropic R_2, correlation time, collagen.

1 | INTRODUCTION

The properties of water in nature are not uniform, which is particularly true in living systems (1). Many highly structured tissues can be found in the human body such as peripheral nerves, white matter, skeletal and myocardial muscles, and tendons and articular cartilage (2,3). Magnetic resonance (MR) imaging, particularly those in characterizing water proton transverse R_2 relaxation and longitudinal $R_{1\rho}$ relaxation in a rotating frame, of these specialized tissues often exhibits an orientation-dependent phenomenon referred to as the magic angle (MA) effect, which could be completely eliminated in a particular $R_{1\rho}$ measurement if the spin-lock (SL) RF power is strong enough (4-7).

The MA effect in cartilage stems exclusively from anisotropic R_2 (i.e. $R_2^q(\theta)$) relaxation that is induced by the restricting reorientation of some water molecules bound to collagen (8-11); thus, a knowledge of $R_2^q(\theta)$ could be indicative of collagen degenerative alterations. As pointed out (7), $R_2^q(\theta)$ could be isolated from one $R_{1\rho}$ dispersion map, which will be computed from images obtained as a function of SL RF power at a constant SL duration (TSL). By contrast, a typical $R_{1\rho}$ relaxation map is derived from images measured as a function of TSL at a constant SL power (12).

The recently proposed composite relaxation metric (R_2-$R_{1\rho}$) for evaluation of cartilage degeneration can be regarded as a simple two-point $R_{1\rho}$ dispersion (13). Similarly, an efficient alternative to R_2-$R_{1\rho}$, ARCADE mapping (14), could be viewed as a one-point $R_{1\rho}$ dispersion. Although it could be measured efficiently (14), $R_2^q(\theta)$ is still only useful for longitudinal studies where the MA effect could be automatically accounted for if cartilage is considered at the same location and the same imaging protocol is followed. In a recent study (15), the pressing need for the MA effect removal

was well demonstrated in which the changes in $R_2^q(\theta)$ triggered by cartilage degeneration were several times smaller than those by the MA effect. Because of this confounding effect, an editorial paper was also published alongside calling for a multidisciplinary effort to eliminate this MA effect for the better evaluation of cartilage degeneration (16).

In the past decade, several techniques have been proposed in which either anisotropic R_2 relaxation was completely suppressed by increasing an echo-time or R_1 relaxation was utilized that had no specific information on collagen integrity (2,6,17). Up to date, it is still an unmet need for developing a novel method to separate the MA effect and yet to maintain the intrinsic sensitivity of anisotropic R_2 to collagen alterations. Therefore, the aim of this work was to develop a theoretical framework in which an Order Parameter wIThout (i.e. reverse "IT") Magic Angle effect (OPTIMA) could be derived from $R_{1\rho}$ dispersion of motion-restricted water in collagen. The proposed order parameter was validated on publicly available ex vivo $R_{1\rho}$ dispersion measured at 9.4T and then demonstrated on one human knee in vivo at 3T.

2 | THEORY

The intramolecular dipolar relaxation rates R_2^{DD} and $R_{1\rho}^{DD}$ of proton pairs in liquid water undergoing isotropic tumbling are usually given by Equations 1-2 (18,19), where d, τ_c, ω_0 and ω_1 denote respectively a constant of $1.028*10^5$ (s^{-1}) for an inter-nuclear distance of 1.59 (Å), a molecular rotational correlation time, an angular Larmor frequency and a SL RF strength.

$$R_2^{DD} = d^2\left\{\frac{3\tau_c}{2} + \frac{2.5\tau_c}{1+\omega_0^2\tau_c^2} + \frac{\tau_c}{1+4\omega_0^2\tau_c^2}\right\} \quad (1)$$

$$R_{1\rho}^{DD} = d^2\left\{\frac{1.5\tau_c}{1+4\omega_1^2\tau_c^2} + \frac{2.5\tau_c}{1+\omega_0^2\tau_c^2} + \frac{\tau_c}{1+4\omega_0^2\tau_c^2}\right\} \quad (2)$$

In biological tissues, water molecules are typically interfacing with many types of macromolecules so that their otherwise unhampered molecular reorientations are markedly hindered and/or slowed down (20).

For MR relaxation studies on these biological tissues (21), it is convenient to categorize water molecular motions into three distinct timescales, i.e. picosecond (ps), nanosecond (ns) and micro- to millisecond (μs-ms). The commonly accessible static

magnetic fields (B_0) for ex vivo and clinical studies are 9.4T or 7.0T and 3.0T; correspondingly, $\omega_1/2\pi$ is usually limited to 2 and 0.5 kHz to prevent any potential RF heating hazards (12). As a result, $R_{1\rho}^{DD}$ will become R_2^{DD} when τ_c is on the ps (i.e. $\omega_0^2\tau_c^2 \ll 1$) or ns (i.e. $\omega_1^2\tau_c^2 \ll 1$) timescale (21). On the other hand, $R_{1\rho}^{DD}$ approximates to $R_2^{DD}/(1+4\omega_1^2\tau_c^2)$ when τ_c is on the μs-ms (i.e. $\omega_0^2\tau_c^2 \gg 1$) timescale because the first terms in Equations 1-2 are the dominant relaxation contributors (14).

In addition to the aforementioned dominant intramolecular dipolar relaxation mechanism, an intermolecular dipolar interaction or a translational diffusion process could also contribute a constant amount (~30%) of the total R_2 or $R_{1\rho}$ on the ps and ns timescales as previously reported (7,21). Moreover, R_2 and $R_{1\rho}$ relaxation can be further enhanced by a different relaxation mechanism named as the chemical exchange (CHEX) effect (22,23), often taking place on the μs-ms timescale. An increase in R_2 due to this mechanism is usually quantified as $R_2^{ex} = p_A p_B \Delta\omega^2(2\tau_{ex})$ (24), where $p_{A/B}$, $\Delta\omega$ and τ_{ex}^{-1} denote respectively molecular fractions, an angular chemical shift difference and an exchange rate between two biological water states (A and B). Note, τ_{ex}^{-1} is redefined here as an average, instead of a sum, of the rate constants of the forward (k_{AB}) and reverse (k_{BA}) reactions. As predicted (24), the CHEX effect on $R_{1\rho}$ would be quenched to $R_2^{ex}/(1+4\omega_1^2\tau_{ex}^2)$, depending directly on ω_1. It is worthwhile to mention that R_2^{ex} can comprise some contributions from water diffusion in the susceptibility-induced field inhomogeneities that might be only relevant at higher B_0 (25).

For the highly ordered tissues such as articular cartilage, the observed R_2 and $R_{1\rho}$ might be summarized using Equations 3-4 (14,21,26),

$$R_2 = R_2^i + R_2^{ex} + R_2^q(\theta) \qquad (3)$$

$$R_{1\rho} = R_2^i + \frac{R_2^{ex}}{1+4\omega_1^2\tau_{ex}^2} + \frac{R_2^q(\theta)}{1+4\omega_1^2\tau_b^2} \qquad (4)$$

where R_2^i, R_2^{ex} and $R_2^q(\theta)$ respectively stand for a *non-specific isotropic* relaxation component including both inter- and intra-molecular dipolar interactions (e.g. molecular rotational and translational diffusions) on the ps and ns timescales (26); a *specific isotropic* relaxation contribution by the CHEX between hydroxyl (-OH) protons in bulk water and in proteoglycans (PG, mostly glycosaminoglycan, GAG) (22) and a *specific*

anisotropic relaxation enhanced by some motion-restricted water undergoing slow (τ_b~ μs-ms) molecular reorientations within a triple-helix microstructure in collagen (9,14,27). Apparently, $R_{1\rho}$ will turn respectively into R_2 or R_2^i when ω_1 is absent or sufficiently strong (i.e. $\omega_1 \gg \tau_b^{-1}$ and τ_{ex}^{-1}).

According to the previous findings (14,27), R_2^{ex} in general hardly contributes more than a few percent of R_2 or $R_{1\rho}$ at 3.0T, which could be attributed primarily to a small chemical shift difference (i.e. $\Delta\omega \approx 1$ ppm) and a slow CHEX rate (i.e., $\tau_{ex}^{-1} \approx$ 1 kHz). Although it is largely insignificant at 3T, R_2^{ex} might need to be reconsidered when $R_2^q(\theta)$ is close to zero at the particular cartilage locations such as in the transitional zone or near the MA orientations (14). Moreover, R_2^{ex} exhibits a quadratic increase with B_0 and thus has the potential to play a significant role at higher B_0 (27). When indeed becoming appreciable, R_2^{ex} could be isolated from the dipolar relaxation by performing either orientation-dependent $R_{1\rho}$ dispersion studies or B_0-dependent R_2 comparisons (27,28).

$R_2^q(\theta)$ in cartilage originates from those preferentially orientated water in collagen (8,10), where a motion-restricted water molecule is "fixed" by two hydrogen bonds connecting with neighboring polypeptide chains in triple-helix interstices (10,11). As a result, an effective <H-H> dipolar interaction vector, as depicted in Figure 1A, tends to align along the principal axis of collagen fibers as simulated by a recent molecular dynamics study on a hydrated collagen model peptide (11). It is customary to quantify $R_2^q(\theta)$ as $R_2^q\langle 3cos^2\theta - 1\rangle^2/4$, where θ is an angle between the collagen fiber direction ($\vec{n}$) and B_0 (+Z) and R_2^q is the maximum of $R_2^q(\theta)$ (9). In this static picture, an effective <H-H> vector is assumed parallel to $\vec{n}$ and the normalized $R_2^q(\theta)$ attains the maximum of 4 or the minimum of zero when θ becomes 0° or the magic angle of ±54.7° as simulated in Figure 1C for collagen fibers in the deep half of cartilage (8). Note, an additional ensemble averaging is required to derive $R_2^q(\theta)$ for those collagen fibers in the superficial half of a femoral cartilage model, resulting in not only less but also different relaxation anisotropy (8,29).

It can be more revealing to depict an illustrative dipolar interaction vector $\overrightarrow{OA}$ in a dynamic picture, assuming an axially symmetric reorientation model as shown in Figure 1B. In this scenario, $\overrightarrow{OA}$ (with an angle of α to B_0) rapidly rotates about a symmetric axis

$\vec{n}$ in collagen fibers at a fixed angle of β, where $\vec{n}$ makes an angle of θ with respect to B_0. Accordingly, a time or an ensemble average $R_2^q(\alpha)$ in Equation 5 could be mathematically transformed into $R_2^q(\theta)$ in Equation 6 by invoking an equality of $\langle 3cos^2\alpha - 1\rangle = \langle 3cos^2\beta - 1\rangle(3cos^2\theta - 1)/2$ (30-32). During this mathematic transformation, the spherical law of cosines (i.e. cosα = cosβ cosθ+ sinβ sinθ cosφ) was employed and both $\langle\cos\varphi\rangle$ and $\langle\cos 2\varphi\rangle$ became zero (30). Note, a time or an ensemble average is indicated by angle brackets and $\tau_\perp$ in Equations 5-6 is an effective correlation time for molecular motion around an axis perpendicular to $\vec{n}$. Consequently, $R_2^q(\theta)$ could be characterized by two terms grouped in two pairs of curly brackets in Equation 6, with the first signifying a residual dipolar interaction constant and the second an orientation-dependent correlation time.

$$R_2^q(\alpha) = \frac{3}{2}\left\{d\frac{\langle 3cos^2\alpha - 1\rangle}{2}\right\}^2 \tau_\perp \quad (5)$$

$$R_2^q(\theta) = \left\{\frac{3}{2}\left(d\frac{\langle 3cos^2\beta - 1\rangle}{2}\right)^2\right\}\left\{\left(\frac{1 - 3cos^2\theta}{2}\right)^2 \tau_\perp\right\} \quad (6)$$

A scaling factor S within the first term in Equation 6, defined as $\langle 3cos^2\beta - 1\rangle/2$, was called an *order parameter* in the literature (33), an intrinsic measure of water molecular reorientation restriction or anisotropy (34). The second term in Equation 6 is directly related to the well-known MA effect, where τ_b, an alternative to $(1 - 3cos^2\theta)^2\tau_\perp/4$, becomes orientation-dependent – a characteristic of an anisotropic molecular motion (35). It was argued that τ_b could have been associated with different processes of breaking and reforming the new hydrogen bonds mediated by the bridged water in collagen triple-helix interstices (32). On the other hand, τ_b could be considered as characterizing a much slower (i.e. $\tau_\perp \gg \tau_\parallel$) molecular reorientation about an axis perpendicular to $\vec{n}$ (14). For this special case, only one correlation time is adequate to characterize the very anisotropic molecular motion otherwise at least two terms are required (36).

Given that $R_2^q(\theta)$ and $\tau_b(\theta)$ could be derived from $R_{1\rho}$ dispersion profile, an order parameter S can be calculated with Equation 7 and the corresponding uncertainty in S can also be determined if the measurement errors in $R_2^q(\theta)$ and $\tau_b(\theta)$ are available. It is worth

underlining that a rotational axis ($\vec{n}$) relative to B_0 could be manipulated arbitrarily by an experimenter in an orientation-dependent relaxation study; however, an intrinsic water bonding property in collagen, rooted in S, should be intact. In other words, $R_2^q(\theta)$ should be directly proportional to $\tau_b(\theta)$ in the orientation-dependent $R_{1\rho}$ dispersion measurements regardless of collagen fiber orientations.

$$S = \sqrt{\frac{2\ R_2^q(\theta)}{3d^2\tau_b(\theta)}} \qquad (7)$$

3 | METHODS

3.1 | $R_{1\rho}$ dispersion acquisitions

3.1.1 | Orientated bovine cartilage specimens: Publicly available $R_2(\theta)$ relaxation and $R_{1\rho}(\theta, \omega_1)$ dispersion datasets were collected by Hänninen et al. of University of Eastern Finland (6) on bovine patellar cartilage samples (n=4) at 9.4T. These samples were identified as *B1S1, B1S2, B1S3* and *B2S3* according to the experiment log files found in the public deposit site (doi:10.5281/zenodo.519752). Seven orientations ($\theta \approx n * 15°$, n=0-6) and four continuous wave (CW) $\omega_1/2\pi$ (0.25, 0.5, 1.0, 2.0 kHz) were employed for the measurements. The pertinent relaxation depth-profiles were extracted and the corresponding angle and depth-profile maps were reprocessed using an included MATLAB script, with a linear interpolation replaced with a spline. Current data analyses were limited to the deep cartilage, defined as an average between 40% and 80% depth. These datasets were intended to validate the predicted correlation between $R_2(\theta)$ and $\tau_b($ $\theta)$.

3.1.2 | Osteoarthritic (OA) human knee specimens: These $R_{1\rho}$ dispersion profiles were measured at 9.4T by Rautiainen et al. of University of Oulu in Finland (37). The average dispersed $R_{1\rho}$ relaxation rates were listed in Table 3 of the original publication for the superficial (SZ), transitional (TZ), radial (RZ) and full (FZ) zones on early (n=5) and advanced (n=9) OA samples, obtained from the tibial plateaus of patients undergoing total knee replacements. Four CW $\omega_1/2\pi$ values (0.125, 0.25, 0.5, 1 kHz) were used in $R_{1\rho}$ dispersion studies and a spin-echo R_2 was treated as a specific $R_{1\rho}$ with $\omega_1/2\pi$ of

zero. The normal to cartilage surface was set approximately parallel to B_0 ($\theta \cong 0°$). These datasets were intended for a sensitivity test for S.

3.1.3 | Enzymatically degraded bovine cartilage: These $R_{1\rho}$ dispersion studies were conducted at 9.4T by Hanni et al. of University of Oulu in Finland (38) on three adjacent subsections in cartilage with and without enzymatic degradations, i.e. Control (CNT), Proteoglycans-digested (GAG-) and Collagen-digested (CA-). Three subsections were taken from the same region in each of intact bovine patellae (n=6). Four CW $\omega_1/2\pi$ values (0.125, 0.25, 0.5, 1 kHz) were used in $R_{1\rho}$ dispersion measurements. Specimens were orientated with articular surfaces perpendicular to B_0. These datasets were used for a specificity test for S.

3.1.4 | Healthy human knee in vivo: One human knee was studied with $R_{1\rho}$ dispersion in the sagittal plane using a 16-Ch T/R Knee Coil (with the maximum possible B_1~$27\mu T$, equivalent to $\omega_1/2\pi$~1.15 kHz) on a 3T MR scanner. Twenty five T1ρ-weighted 3D images were acquired using a SL-prepared T1-enhanced 3D TFE pulse sequence, with varying TSLs (1, 10, 20, 30 and 40 ms) and $\omega_1/2\pi$ (0.125, 0.25, 0.5, 0.75, 1.0 kHz). The SL was self-compensated using the rotary echo scheme (39). The specific absorption rate (SAR) of $R_{1\rho}$ pulse sequence with the longest TSL and the highest ω_1 was about 45% less than the allowed maximum local extremities value (20 W/Kg) in the normal operating mode.

Each T1ρ-weighted 3D image dataset was collected in an interleaved segmented elliptical centric encoding scheme in k-space (40). There were 52 shots in total with each collecting 64 profiles, and a shot interval was 2000 ms. Each profile was collected with TR/TE of 8.5/4.3 ms and RF flip angle of 10°. An acquisition bandwidth was 382 Hz and fat signal was suppressed with binomial 1-2-1 pulses.

The field of view (FOV) was 130 by 130 by 96 mm^3 with an acquired voxel size of 0.40*0.40*3.00 mm^3. With a compressed SENSE (41) reduction factor of 3, each dataset took 1.75 minutes leading to the total scan duration of about 45 minutes. This in vivo study aimed at a feasibility test in a clinical setting.

3.2 | $R_{1\rho}$ dispersion modeling

3.2.1 | Orientated bovine cartilage specimens: S was derived after R_2^{ex} had been removed from $R_{1\rho}(\theta, \omega_1)$ as shown in a workflow chart in Figure 2C. Specifically, the minimum of $R_2(\theta)$ expressed by $R_2^q\langle 3cos^2(\theta+\delta)-1\rangle^2/4)$ was first determined using Equation 3, identifying a measured magic angle θ_{MA} and a sum of R_2^i and R_2^{ex}. In this step, the orientation-dependence curve was allowed to float an angle δ within a limited range to account for any potential errors in positioning samples or an intrinsic deviation of deep collagen fibers from an assumed perpendicular orientation to articular surface (6).

Then, a specific $R_{1\rho}(\theta_{MA}, \omega_1)$ dispersion was modeled using Equation 4 excluding $R_2^q(\theta)$, separating R_2^{ex} from R_2^i. Next, $R_{1\rho}(\theta, \omega_1)$ dispersion was fitted using Equation 4 without R_2^{ex} for each orientation θ except for those near θ_{MA}; accordingly, an individual $S(\theta)$ was computed with Equation 7 for each pair of the fitted $R_2^q(\theta)$ and $\tau_b(\theta)$. Last, an average S and its standard deviation were calculated for each of four samples from those $S(\theta)$ derived from different sample orientations.

3.2.2 | OA human knee specimens: With a simplified $R_{1\rho}$ dispersion model, $R_2^q(\theta\cong 0)$ and $\tau_b(\theta\cong 0)$ with the uncertainties of ΔR_2^q and $\Delta\tau_b$ were determined using Equation 4 without R_2^{ex}. S was then calculated based on Equation 7, and the relative uncertainty in S (i.e. $\Delta S/S$) was estimated as $0.5*\sqrt{\left(\Delta R_2^q/R_2^q\right)^2+\left(\Delta\tau_b/\tau_b\right)^2}$.

3.2.3 | Enzymatically degraded bovine cartilage samples: The modeled $\tau_b(\theta\cong 0)$ and $R_2^q(\theta\cong 0)$ were respectively listed and shown in Table 1 and Figure 1 for the superficial (5% depth) and full (100% depth) cartilage zones from the original publication (38). The precise R_2^q values and their uncertainties were kindly provided (private communication with Dr. Matti Hanni of University of Oulu). Therefore, S and its uncertainty could be computed as aforementioned.

3.2.4 | Healthy human knee in vivo: $R_{1\rho}$-weighted 3D images were first co-registered following an established protocol and $R_{1\rho}$ pixel maps were then generated by fitting the aligned images to a two-parameter exponential decay model using different ω_1 (14). Next, different cartilaginous tissues were angularly and radially segmented (42) and an ROI-based $R_{1\rho}$ dispersion profile in the deep zone was modeled with Equation 4 without

R_2^{ex}. Last, an average S and its descriptive statistics were calculated for each cartilage compartment.

3.3 | Nonlinear least-squares curve fitting

The curve fittings for R_2 orientation-dependence and $R_{1\rho}$ dispersion in Equations 3-4 were carried out using a publicly available IDL script that relies on the Levenberg-Marquardt technique (http://purl.com/net/mpfit) (43). As the fits were unweighted, the output formal 1-sigma fitting errors had been scaled so that the obtained reduced chi-squared χ^2 values were close to unity. The searching ranges were constrained for the model parameters: δ = [-30°,30°]; R_2^{ex} = [0, 30] (1/s); τ_{ex} and τ_b= [10^1, 10^4] (μs); R_2^i =[0, 30] (1/s); R_2^a = [0, 300] or [0, 30] (1/s) for ex vivo or in vivo data, respectively. If the fitted parameters were equal to the boundary values or their relative uncertainties were larger than 300%, these fits were deemed to be failed and thus had been excluded from further analysis.

3.4 | Statistical analysis

The differences and correlations between any two relaxation metrics were quantified using the Student's t-test (a two-tailed distribution) and the Pearson correlation coefficient (r), with the statistical significance considered at $P < 0.05$. Inter-group comparisons were visualized using box-and-whisker and bar plots, and the correlations were presented in scatterplots overlaid with 95% confidence level data ellipses for an enhanced visualization (44). All measurements are shown as mean ± SD unless stated otherwise, and all image and data analysis were conducted with an in-house software developed in IDL 8.5 (Harris Geospatial Solutions, Inc., Broomfield, CO, USA).

4 | RESULTS

4.1 | Orientated bovine cartilage specimens

Two orientation-dependent relaxation depth-profile maps are reproduced in Figure 2 for T_2 (A) and $T_{1\rho}$ (B) with $\omega_1/2\pi$ of 2 kHz from one sample (B1S2) (6). The MA effect can be recognized in the deep cartilage when orientated near 60° relative to B_0 (A); however, this R_2 ($1/T_2$) anisotropy was largely quenched in $R_{1\rho}$ ($1/T_{1\rho}$) with a larger ω_1 (B) as previously reported (5).

The logic of the following data analysis was provided by a workflow chart (Figure 2C). As shown in Figure 3A, three orientation-dependent $R_{1\rho}$ were modeled

(solid lines) for the measured averages (dashed lines) with $\omega_1/2\pi$ (kHz) of 0 (red), 0.25 (green), and 2.0 (blue). Included also are an example of separating R_2^{ex} (Figure 3B) and an example of modeling $R_{1\rho}$ dispersion (Figure 3C).

A magic angle θ_{MA} of 59.6±0.3° was fitted with Equation 3 when R_2 ($\omega_1/2\pi$=0) at the minimum (Figure 3A). $R_{1\rho}$ dispersion at θ_{MA} was then modeled using Equation 4 (Figure 3B), resulting in a dispersed R_2^{ex} of 5.6 $\pm$ 0.2 (1/s), a constant isotropic R_2^i of 10.4 $\pm$ 0.2 (1/s) and τ_{ex} of 161.7±12.9 (μs). After eliminating R_2^{ex}, a typical (θ=20°) $R_{1\rho}$ dispersion was best characterized using Equation 4 with a dominant R_2^q of 86.3±5.3 (1/s), a minor constant R_2^i of 11.3±3.3 (1/s) and τ_b of 459.0±28.7 (μs) (Figure 3C).

Table 1 summarizes the partitioned R_2 absolute (1/s) and relative (%) relaxation rates, θ_{MA}, τ_{ex} (μs), $\langle R_2^q(\theta)\rangle$ and $\langle \tau_b(\theta)\rangle$ denoting data ellipse centroids, and an average S for each of four samples. The largest and smallest average S values as seen in Figure 4B were related respectively to the largest and smallest ratios of $\langle R_2^q(\theta)\rangle$ and $\langle \tau_b(\theta)\rangle$ for B1S3 and B1S2. As noted (6), θ_{MA} was not exactly equal to the theoretical value of 54.7° but differed on average by about 10°. Accordingly, an average S was determined only from those sample orientations in which $R_{1\rho}$ relaxation underwent substantial dispersion, i.e. θ < 50° (B1S1 and B2S3) or 35° (B1S2 and B1S3).

An anisotropic R_2^q and an isotropic R_2^{ex} generally contributed the most (~90%) and the least (~3%) to the total R_2, in good agreement with the literature (7,27). More importantly, $\tau_b(\theta)$ demonstrated on average a significantly high correlation (r = 0.89 $\pm$ 0.05, P < 0.05) with $R_2^q(\theta)$ as demonstrated in Figure 4A, in accordance with the predicted from this work. An average S was then compared for each sample in Figure 4B, revealing a smaller intra-sample variation compared to an inter-sample one, i.e. 9.5% vs. 22.8%.

4.2 | OA human knee specimens

Figure 5A presents the observed (symbols) and the modeled (lines) contrasting $R_{1\rho}$ dispersion profiles (37) in the superficial (SZ, solid lines) and radial (RZ, dashed lines) zones for early (blue) and advanced (red) OA specimens. The differences in $R_{1\rho}$ between two OA grades tend to decrease as ω_1 increases, indicating that the cartilage degenerative

changes are best characterized by an anisotropic R_2^a rather than an isotropic R_2^i. It is worthwhile to mention that R_2^a in RZ (empty symbols) was much larger than those in SZ (filled symbols) as previously documented (4,6).

Table 2 summarizes the $R_{1\rho}$ dispersion modeling results (R_2^i, R_2^a, τ_b and S) for different cartilage compartments with two OA grades. As shown in Figure 5B, S (10^{-3}) from early OA was significantly larger than that from advanced OA particularly in SZ (i.e. 1.89±0.05 vs. 1.01±0.04, $P < 0.001$). This observation indicated that the integrity of collagen microstructure had been further compromised in advanced OA.

4.3 | Enzymatically degraded bovine cartilage samples

The $R_{1\rho}$ dispersion modeling results for the selectively modified cartilage samples are also tabulated in Table 2. The observed S alterations after enzymatic depletions in two cartilage zones are compared in Figure 5C. With regard to CNT, the water ordering/bonding capacity in SZ (5% depth, yellow) was more disrupted when comparing CA- to GAG-depleted samples.

Specifically, S exhibited no difference between GAG- and CNT (1.23 ± 0.09 vs. 1.28 ± 0.05, $P = 0.262$); however, it clearly revealed a significant difference between CA- and CNT (0.64 ± 0.01 vs. 1.28 ± 0.05, $P < 0.001$). A similar trend was observed when $R_{1\rho}$ dispersion was measured on the whole cartilage (100% depth, blue). Note, the $R_{1\rho}$ dispersion model used in the original work (38) was the same as Equation 4 without R_2^{ex}.

4.4 | Healthy human knee in vivo

Figure 6B shows three ROI-based $R_{1\rho}$ dispersion profiles (colored lines) from the femoral (red), tibial (green) and patellar (blue) cartilage deep zones, highlighted by colored arrows on one $R_{1\rho}$-weighted ($\omega_1/2\pi$=1 kHz, TSL=1 ms) image slice (Figure 6A). The maximum and minimum of R_2, i.e. $R_{1\rho}$ with $\omega_1/2\pi$ of zero, were respectively found in the tibial and femoral cartilage compartments, consistent with the theoretical prediction as the collagen fibers from these two ROIs were nearly parallel or at the MA to B_0 (8,9).

Noticeably, $R_{1\rho}$ dispersion modeling was only successful for the highlighted ROIs in the tibial or the patellar but not in the femoral compartment; specifically, the fitted R_2^i (1/s), R_2^a(1/s) and τ_b (μs) values were 12.9 ± 0.3; 11.0 ± 0.2 and 148 ± 6.1 in the tibial

and 6.7 ± 9.1; 14.2 ± 8.0 and 134.4 ± 132.7 in the patellar cartilage. The overall qualities of $R_{1\rho}$ dispersion data from this particular image slice could be appreciated in Figure 6C-E for all segmented ROIs in the femoral (C), tibial (D) and patellar (E) locations, showing some unexpected $R_{1\rho}$ dispersion profiles particularly when using a weak ω_1.

The total numbers of the segmented ROIs in the femoral, tibial and patellar cartilage from all image slices were 466, 55 and 50; however, only 52%, 61% and 76% of those were successfully modeled. The descriptive statistics for $R_{1\rho}$ dispersion profiles (measured and modeled) and the derived S are summarized in Table 3. As ω_1 increased, the average $R_{1\rho}$ and its variation would decrease, indicating that $R_2^q(\theta)$ had been progressively quenched as previously reported (5,6).

Compared with the derived R_2^q, R_2^i became more clustered indicated by a relatively smaller standard deviation, e.g. 11.7±2.9 vs.11.3±4.9 (1/s) in the femoral cartilage, and the same trend could also be found in Figure 5A. More importantly, $\tau_b(\theta)$ were positively correlated (r = 0.48, P < 0.001) with $R_2^q(\theta)$ for all cartilage compartments as demonstrated in Figure 7A. Subsequently, the derived S (10^{-3}) statistics from each cartilage location were compared in Figure 7B, showing no significant differences between the tibial (1.82±0.64) and the femoral (1.74±0.53, $P = 0.49$) or the patellar (1.97±0.33, $P = 0.21$) cartilage. However, a significant ($P < 0.01$) difference was observed between the femoral and the patellar cartilage.

5 | DISCUSSION

5.1 | General comments: A theoretical framework has been formulated in this work to derive an orientation-independent MR metric in ordered tissue, which was verified and demonstrated for its sensitivity, specificity and feasibility. The preliminary results show that the introduced order parameter could be a potentially useful MR biomarker for collagen alterations in cartilage and other highly organized tissues. To the best of our knowledge, this is the first effort to separate the MA effect from MR relaxation without loss of intrinsic water ordering information in cartilage.

5.2 | An order parameter for restricted molecular reorientation: Water proton relaxation in biological tissues had been thoroughly studied in the past (20,21); however, an additional anisotropic dipolar relaxation contribution has to be included to better

characterize R_2 in highly ordered tissues such as articular cartilage, and this particular contribution could be quenched as expressed in Equations 3-4 (14).

It is not straightforward to comprehend the biophysical relaxation mechanism for an anisotropic relaxation (7). As previously reported (7,27), $R_{1\rho}$ dispersion was predominantly induced by the anisotropic dipolar interaction of water molecules associated with collagen and the CHEX effect would only contribute appreciably at higher B_0. The measured relaxation contributions to R_2 as reported in Table 1 are in line with previous findings (27).

When deriving S, we have drawn an analogy between the magic angle spinning (MAS) in solid NMR and water preferential alignments in collagen (30). As a result, the related theoretical backgrounds used for developing the MAS technique can be equally applied to the anisotropic molecular reorientations in collagen, resulting in the separated MA effect from a residual dipolar coupling constant.

5.3 | A theory validation on orientated cartilage: Because of diminishing $R_{1\rho}$ dispersion near MA orientations, an average S was only derived from limited sample orientations, which could be partially responsible for the reported varying standard deviation in S and the observed non-zero x-intercepts inferred from the data ellipse orientations. It is interesting to note that the sample B1S1 presented almost no x-intercept in Figure 4A and it happened to have more data points for calculating S because of the unusual sample orientations with θ_{MA} close to 80° (see Table 1). On the other hand, the average S values were substantially different among four samples, possibly due to the varied internal (e.g. cartilage location, animal age) or external factors (e.g. hydration, temperature).

It was somewhat unexpected that the estimated R_2^{ex} hardly (~3%) contributed to R_2 in bovine cartilage at 9.4T, given that ~15-20% R_2 increase was reported at 7T compared to 3T for human knee cartilage. While the reported R_2^{ex} estimates were derived from R_2 measurements at 3T and 7T, our estimates were based on $R_{1\rho}$ dispersion at θ_{MA} that might be compromised by some systematic errors.

Had both the collagen fibers and B_0 been perpendicular to the cartilage surface, the minimum R_2 should have been detected around θ_{MA} of 54.7°. Yet, an average

"apparent" θ_{MA} measured in this study was offset by about 10° (6), implying that either B_0 and/or collagen fibers in the deep zone were not exactly perpendicular to the cartilage surface.

5.4 | Evaluating sensitivity and specificity ex vivo: The most sensitive relaxation parameter was reportedly the one with the highest orientation anisotropy (6), which was clearly supported by the experimental data in Figure 5A when comparing an anisotropic R_2^a ($\omega_1 = 0$) with an isotropic R_2^i ($\omega_1 \to \infty$) for early and advanced OA samples. Recently, τ_b was proposed as a promising novel biomarker for the evaluation of cartilage degeneration (38). The final outcome of the these evaluations using either R_2^a or τ_b would have been different had the samples been orientated differently. In this regard, the proposed new metric could be advantageous and it had been validated not only sensitive to the OA grades but also specific to collagen degradation.

5.5 | Measuring an order parameter in vivo: Due to the lengthy in vivo imaging protocol, it was likely that the observed $R_{1\rho}$ dispersion had been compromised by the motion or blurring artifacts (14). Furthermore, the quantitative accuracy of $R_{1\rho}$dispersion could be further compounded by an inconsistent spin-locking and an imperfect imaging pulse sequence (40). In this work, a smaller RF flip angle of 10◦ and a shorter TR of 8.3 ms, relative to R_1 of 1240 ms in cartilage at 3T (45), were used to partially mitigate these potential systematic errors.

Not all segmented ROIs could be optimally modeled in this work. Had the stricter criterion been used to define a successful fit, the overall successful rates would have been reduced, suggesting that $R_{1\rho}$ dispersion data had possibly been impaired by imaging artifacts. To some extent, an imperfect imaging protocol could account for why some curve-fittings were not successful. However, a diminishing $R_{1\rho}$ dispersion near the MA locations was probably the primary reason contributing to a lower successful rate in the femoral (35%) compared to in the tibial (49%) cartilage.

Relatively large S variations in human knee cartilage in vivo were observed, which might be induced by intrinsically different biomechanical properties at various cartilage locations such as weight-bearing and non-weight-bearing areas. Preferentially oriented water in collagen plays a crucial, and yet not fully understood, role in

biomechanics of cartilage (46); hence, S might be served as an indicator for varying biomechanical functions among different cartilaginous joint tissues. For instance, $S(10^{-3})$ was about 2 for human knee cartilage in vivo (Figure 7B) compared with that of around 4 for bovine patellar cartilage (Figure 4B), and that of about 35 for the cartilage in hydrated (~25%) bovine Achilles tendon (33).

5.6 | Limitations and future work: Several limitations to this work need to be acknowledged. First, only a limited number of cartilage samples and human knee in vivo were examined and thus the reported statistical analysis might be biased. Second, the proposed method might become less reliable for some femoral cartilage near the MA locations. Third, the $R_{1\rho}$ dispersion acquisition strategy for human knee in vivo was by no means the best of choice and the lengthy scan duration could have contributed to the considerable variations to the reported order parameters. Last, there was no "gold standard" to which the derived order parameter could be compared in vivo; therefore, a direct association between the measured and the physical reality could not be confirmed.

Before undertaking in vivo validations on a large cohort of subjects, a few technical challenges must be overcome in designing an efficient and reliable $R_{1\rho}$ dispersion acquisition strategy. Up to date, none of the existing spin-locking pulses is suitable for quantitative $R_{1\rho}$ dispersion investigations due to their sensitivities to B_1 and B_0 field artifacts when using a larger range of ω_1 (47,48). Neither was the reported phase cycling strategy (40) optimal for improving $R_{1\rho}$ quantitative accuracy as it would have doubled the scan time if this method had been implemented in our imaging pulse sequence. Further work is underway to develop an efficient $R_{1\rho}$ dispersion imaging protocol suitable for clinical studies; hopefully, it will facilitate a thorough validation of the proposed novel MR metric on human knee in vivo and expand to other highly organized tissues.

6 | CONCLUSIONS

We have developed a theoretical framework and applied it to both ex vivo and in vivo studies on articular cartilage. The preliminary results from these studies demonstrate that an orientation-independent order parameter could be derived from $R_{1\rho}$ dispersion, both sensitive and specific to the integrity of microstructure in collagen. It is foreseen that the

developed method will probably broaden the current spectrum of the compositional MR imaging applications on articular cartilage and other highly ordered tissues.

ACKNOWLEDGEMENTS

The author would like to thank Drs. Nina Hänninen (University of Eastern Finland, Kuopio, Finland) and Matti Hanni (University of Oulu, Oulu, Finland) for sharing their ex vivo $R_{1\rho}$ dispersion data. The unknown referee's valuable and profound comments are greatly appreciated. This work would not have been possible without the support and encouragement from Prof. Thomas Chenevert. Research reported here was partially supported by the Eunice Kennedy Shriver National Institute of Child Health & Human Development of the National Institutes of Health under Award Number R01HD093626 (to Prof. Riann Palmieri-Smith). The content is solely the responsibility of the author and does not necessarily represent the official views of the National Institutes of Health.

REFERENCES

1. Ball P. Water is an active matrix of life for cell and molecular biology. Proceedings of the National Academy of Sciences 2017;114(51):13327-13335.
2. Bydder M, Rahal A, Fullerton GD, Bydder GM. The magic angle effect: a source of artifact, determinant of image contrast, and technique for imaging. J Magn Reson Imaging 2007;25(2):290-300.
3. Henkelman RM, Stanisz GJ, Kim JK, Bronskill MJ. Anisotropy of NMR properties of tissues. Magn Reson Med 1994;32(5):592-601.
4. Xia Y. Magic-angle effect in magnetic resonance imaging of articular cartilage: a review. Invest Radiol 2000;35(10):602-621.
5. Akella SV, Regatte RR, Wheaton AJ, Borthakur A, Reddy R. Reduction of residual dipolar interaction in cartilage by spin-lock technique. Magn Reson Med 2004;52(5):1103-1109.
6. Hanninen N, Rautiainen J, Rieppo L, Saarakkala S, Nissi MJ. Orientation anisotropy of quantitative MRI relaxation parameters in ordered tissue. Sci Rep 2017;7(1):9606.

7. Borthakur A, Mellon E, Niyogi S, Witschey W, Kneeland JB, Reddy R. Sodium and T1ρ MRI for molecular and diagnostic imaging of articular cartilage. NMR Biomed 2006;19(7):781-821.
8. Berendsen HJC. Nuclear magnetic resonance study of collagen hydration. J Chem Phys 1962;36(12):3297-3305.
9. Momot KI, Pope JM, Wellard RM. Anisotropy of spin relaxation of water protons in cartilage and tendon. NMR Biomed 2010;23(3):313-324.
10. Fullerton GD. The magic angle effect in NMR and MRI of cartilage. In: Xia Y, Momot KI, editors. Biophysics and Biochemistry of Cartilage by NMR and MRI. Cambridge, UK: The Royal Society of Chemistry; 2016. p 109-144.
11. Tourell MC, Momot KI. Molecular dynamics of a hydrated collagen peptide: insights into rotational motion and residence times of single-water bridges in collagen. J Phys Chem B 2016;120(49):12432-12443.
12. Wang L, Regatte RR. T(1)rho MRI of human musculoskeletal system. J Magn Reson Imaging 2015;41(3):586-600.
13. Russell C, Pedoia V, Majumdar S, Consortium A-A. Composite metric R2 - R1rho (1/T2 - 1/T1rho) as a potential MR imaging biomarker associated with changes in pain after ACL reconstruction: A six-month follow-up. J Orthop Res 2017;35(3):718-729.
14. Pang Y, Palmieri-Smith RM, Malyarenko DI, Swanson SD, Chenevert TL. A unique anisotropic R2 of collagen degeneration (ARCADE) mapping as an efficient alternative to composite relaxation metric (R2 -R1 rho) in human knee cartilage study. Magn Reson Med 2019;81(6):3763-3774.
15. Shao H, Pauli C, Li S, Ma Y, Tadros AS, Kavanaugh A, Chang EY, Tang G, Du J. Magic angle effect plays a major role in both T1rho and T2 relaxation in articular cartilage. Osteoarthritis Cartilage 2017;25(12):2022-2030.
16. Roemer FW, Kijowski R, Guermazi A. Editorial: from theory to practice - the challenges of compositional MRI in osteoarthritis research. Osteoarthritis Cartilage 2017;25(12):1923-1925.

17. Ma YJ, Shao H, Du J, Chang EY. Ultrashort echo time magnetization transfer (UTE-MT) imaging and modeling: magic angle independent biomarkers of tissue properties. NMR Biomed 2016;29(11):1546-1552.
18. Abragam A. The principles of nuclear magnetism. Oxford: Clarendon Press; 1961. 599 p.
19. Jones GP. Spin-lattice relaxation in the rotating frame: weak-collision case. Physical Review 1966;148(1):332-335.
20. Mathur-De Vre R. The NMR studies of water in biological systems. Progress in Biophysics and Molecular Biology 1980;35:103-134.
21. Knispel RR, Thompson RT, Pintar MM. Dispersion of proton spin-lattice relaxation in tissues. J Magn Reson 1974;14(1):44-51.
22. Duvvuri U, Goldberg AD, Kranz JK, Hoang L, Reddy R, Wehrli FW, Wand AJ, Englander SW, Leigh JS. Water magnetic relaxation dispersion in biological systems: The contribution of proton exchange and implications for the noninvasive detection of cartilage degradation. P Natl Acad Sci USA 2001;98(22):12479-12484.
23. Wang P, Block J, Gore JC. Chemical exchange in knee cartilage assessed by R1rho (1/T1rho) dispersion at 3T. Magn Reson Imaging 2015;33(1):38-42.
24. Fischer MWF, Majumdar A, Zuiderweg ERP. Protein NMR relaxation: theory, applications and outlook. Progress in Nuclear Magnetic Resonance Spectroscopy 1998;33:207-272.
25. Spear JT, Gore JC. New insights into rotating frame relaxation at high field. NMR Biomed 2016;29(9):1258-1273.
26. Reddy R, Borthakur A, Witschey WR, Kneeland JB. Frontiers in molecular imaging of cartilage: Future developments. Cartilage Imaging: Springer; 2011. p 213-227.
27. Mlynarik V, Szomolanyi P, Toffanin R, Vittur F, Trattnig S. Transverse relaxation mechanisms in articular cartilage. J Magn Reson 2004;169(2):300-307.
28. Pang Y. Toward an orientation-independent MR relaxation metric from R1ρ dispersion in articular cartilage. In: Proceedings of the 27th Annual Meeting of ISMRM, Montreal, Quebec, Canada, 2019. (abstract 1325).

29. Grunder W. MRI assessment of cartilage ultrastructure. NMR Biomed 2006;19(7):855-876.
30. Hennel JW, Klinowski J. Magic-angle spinning: a historical perspective. New techniques in solid-state NMR: Springer; 2005. p 1-14.
31. Woessner DE. Nuclear magnetic-relaxation and structure in aqueous heterogenous systems. Mol Phys 1977;34(4):899-920.
32. Peto S, Gillis P, Henri VP. Structure and dynamics of water in tendon from NMR relaxation measurements. Biophysical journal 1990;57(1):71-84.
33. Lenk R, Bonzon M, Greppin H. Dynamically oriented biological water as studied by NMR. Chemical Physics Letters 1980;76(1):175-177.
34. Fechete R, Demco D, Blümich B. Order parameters of the orientation distribution of collagen fibers in Achilles tendon by 1H NMR of multipolar spin states. NMR Biomed 2003;16(8):479-483.
35. Woessner DE, Snowden Jr BS. Magnetic relaxation under hindered rotation in fluids. Advan Mol Relaxation Processes 1972;3:181-197.
36. Woessner DE, Zimmerman JR. Nuclear transfer and anisotropic motional spin phenomena - relaxation time temperature dependence studies of water adsorbed on silica gel .4. J Phys Chem-Us 1963;67(8):1590-1600.
37. Rautiainen J, Nissi MJ, Salo EN, Tiitu V, Finnila MAJ, Aho OM, Saarakkala S, Lehenkari P, Ellermann J, Nieminen MT. Multiparametric MRI assessment of human articular cartilage degeneration: Correlation with quantitative histology and mechanical properties. Magn Reson Med 2015;74(1):249-259.
38. Hanni M, Nissi MJ, Rautiainen J, Saarakkala S, Ellermann J, Nieminen MT. Determination of correlation time in articular cartilage by T1rho relaxation dispersion. In: Proceedings of the 23rd Annual Meeting of ISMRM,Toronto, OntarioI, Canada, 2015. (abstract 0117).
39. Charagundla SR, Borthakur A, Leigh JS, Reddy R. Artifacts in T-1 rho-weighted imaging: correction with a self-compensating spin-locking pulse. J Magn Reson 2003;162(1):113-121.

40. Li X, Han ET, Busse RF, Majumdar S. In vivo T(1rho) mapping in cartilage using 3D magnetization-prepared angle-modulated partitioned k-space spoiled gradient echo snapshots (3D MAPSS). Magn Reson Med 2008;59(2):298-307.
41. Geerts-Ossevoort; L, Weerdt; Ed, Duijndam; A, IJperen; Gv, Peeters; H, Doneva; M, Nijenhuis; M, Huang A. Compressed SENSE. Speed done right. Every time. https://philipsproductcontent.blob.core.windows.net/assets/20180109/619119731f2a42c4acd4a863008a46c7.pdf. Philips Healthcare; 2018.
42. Kaneko Y, Nozaki T, Yu H, Chang A, Kaneshiro K, Schwarzkopf R, Hara T, Yoshioka H. Normal T2 map profile of the entire femoral cartilage using an angle/layer-dependent approach. J Magn Reson Imaging 2015;42(6):1507-1516.
43. Markwardt CB. Non-linear least-squares fitting in IDL with MPFIT. Astronomical Data Analysis Software and Systems XVIII ASP Conference Series 2009;411:251.
44. Friendly M, Monette G, Fox J. Elliptical insights: understanding statistical methods through elliptical geometry. Stat Sci 2013;28(1):1-39.
45. Gold GE, Han E, Stainsby J, Wright G, Brittain J, Beaulieu C. Musculoskeletal MRI at 3.0 T: relaxation times and image contrast. American Journal of Roentgenology 2004;183(2):343-351.
46. Bella J. Collagen structure: new tricks from a very old dog. Biochem J 2016;473:1001-1025.
47. Chen W. Errors in quantitative T1rho imaging and the correction methods. Quant Imag Med Surg 2015;5(4):583-591.
48. Mitrea BG, Krafft AJ, Song RT, Loeffler RB, Hillenbrand CM. Paired self-compensated spin-lock preparation for improved T-1 rho quantification. J Magn Reson 2016;268:49-57.

SEVEN FIGURE CAPTIONS

FIGURE 1 An illustrative intramolecular dipolar interaction vector H-H (red) in bridged water and an ensemble-averaged (black) vector < H-H > along a triple-helix model peptide (A) as simulated by a molecular dynamics study (Reprinted with permission from Reference 11. Copyright © 2016, American Chemical Society). The average <H-H> vector ($\overrightarrow{OA}$), with an angle of α to B_0 (+Z) as shown in Figure 1B, rotates at an angle of β around an axially symmetric axis in collagen fibers ($\vec{n}$) that in turn forms an angle of θ to B_0 (+Z). The time-dependent angles are α and φ. The orientation-dependence of the normalized anisotropic $R_2(\theta)$ were simulated in Figure 1C for the superficial and deep halves of model femoral cartilage.

FIGURE 2 Two representative orientation-dependent depth-profile maps of T_2 (A) relaxation times (ms) and $T_{1\rho}$ relaxation times (ms) with a spin-lock RF strength ($\omega_1/2\pi$) of 2 kHz (B) measured on one bovine cartilage sample (B1S2) (Reproduced from the publicly available data in Reference 6). A horizontal depth-profile starts from the articular surface (0%) to the bone interface (100%) and the deep zone was defined as reported between 40% and 80% in depth, highlighted with two vertical dashed lines (B). A workflow chart (C) is included to guide the perspective readers better following the data analysis.

FIGURE 3 Three orientation-dependent $R_{1\rho}$ (1/s) relaxation profiles with $\omega_1/2\pi$ of 0 (red), 0.25 (green) and 2 kHz (blue) for the same sample B1S2 (A), with solid lines standing for best fits to $R_2^q(3cos^2\theta - 1)^2/4$ for the averages measured in the deep cartilage indicated by the dashed lines in the middle of shaded areas (i.e. ±standard deviations). Two specific $R_{1\rho}$ (1/s) dispersion profiles induced respectively by chemical exchange effect (θ=60°) and by residual dipolar interaction (θ=20°) are demonstrated in Figure 3B-C.

FIGURE 4 A scatterplot showing the positive correlations between $R_2^q(\theta)$ (1/s) and τ_b (μs) from the orientation-dependent $R_{1\rho}$ dispersion measurements (A) and the box-and-whisker plot comparing the derived order parameter S (10^{-3}) among four bovine cartilage samples (B).

FIGURE 5 For early (blue) and advanced (red) osteoarthritis (OA) in human knee specimens (A-B), the measured (symbols) and modeled (lines) $R_{1\rho}$ dispersion profiles at 9.4T are shown for the superficial (SZ, solid lines) and radial (RZ, dashed lines) cartilage zones (A). The derived order parameters S (10^{-3}) are compared in B. For enzymatically depleted bovine patellae samples (C), the derived S (10^{-3}) are compared among the control (CNT), proteoglycan-depleted (GAG-) and collagen-depleted (CA-) within 5% (yellow) and 100% (blue) cartilage zonal depth at 9.4T.

FIGURE 6 A representative $R_{1\rho}$-weighted image slice ($\omega_1/2\pi$=1 kHz, TSL=1 ms) with angularly and radially segmented ROIs overlaid (A). Three ROIs are highlighted by colored arrows in the femoral (red), tibial (green) and patellar (blue) compartments and the corresponding $R_{1\rho}$ dispersion profile (filled symbols) and modeling (solid and dashed lines) are plotted (B). The orientation-dependent $R_{1\rho}$ dispersion profiles of all segmented ROIs are presented for the femoral (C), tibial (D) and patellar (C) cartilage. Note, the orientation angles for the tibial ($\emptyset$=0°) and patellar ($\emptyset$=90°) compartments are just for an annotation purpose, and the dashed-lines indicate the specific $R_{1\rho}$ dispersion profiles shown in B.

FIGURE 7 A scatterplot (A) of anisotropic $R_2^a(\theta)$ (1/s) and correlation time $\tau_b(\mu s)$, and a box-and-whisker diagram (B) of the order parameters S (10^{-3}) derived from the femoral (red circles), tibial (green squares) and patellar (blue triangles) compartments in an asymptomatic adult knee at 3T.

THREE TABLES

TABLE 1 $R_{1\rho}$ dispersion model parameters in the deep zone of four bovine patellar cartilage specimens at 9.4T. The absolute (1/s) and relative (%) rates are for the maximum anisotropic R_2^a, isotropic R_2^i and chemical exchange contribution R_2^{ex}. Others include the measured magic angles θ_{MA} (°), chemical exchange correlation times τ_{ex} (μs), average residual dipolar interaction correlation times $\langle \tau_b(\theta) \rangle$ (μs), average anisotropic $\langle R_2^a(\theta) \rangle$ (1/s) and average order parameters S. All data are reported as mean ± standard deviation.

	R_2^a	R_2^i	θ_{MA}	R_2^{ex}	τ_{ex}	$\langle \tau_b(\theta) \rangle$	$\langle R_2^a(\theta) \rangle$	S (10^{-3})
B1S1	98.3±1.7 (88%)	10.1±0.3 (9%)	77.6±0.3	3.8±0.4 (3%)	192.4±42.5	251.1±65.7	67.6±23.2	4.09±0.28
B1S2	147.5±2.4 (90%)	10.4±0.2 (6%)	59.6±0.3	5.6±0.2 (3%)	161.7±12.9	523.8±27.3	83.5±18.2	3.15±0.28
B1S3	185.1± 2.0 (93%)	11.1±1.2 (6%)	58.5±0.1	3.4±1.3 (2%)	115.4±85.4	355.2±28.3	146.0±20.5	5.08±0.24
B2S3	103.1±0.6 (88%)	10.0±0.5 (9%)	61.8±0.1	3.7±0.8 (3%)	293.4±120.1	367.8±18.5	65.7±23.1	3.29±0.57
AVE	133.5±35.4 (90%)	10.4±0.4 (7%)	64.4±8.9	4.1±0.9 (3%)	190.7±65.3	374.5±112.5	90.7±37.7	3.90±0.89

TABLE 2 $R_{1\rho}$ dispersion model parameters from different cartilage zones in osteoarthritic (OA) human knee samples (early vs. advanced OA) and enzymatically depleted bovine cartilage specimens at 9.4T. SZ, RZ and FZ denote respectively the superficial, radial and full cartilage zones; CNT, GAG- and CA- represent respectively the control, proteoglycans-depleted and collagen-depleted samples. All data are reported as mean ± standard deviation.

	Human Knee Tibial Cartilage Samples at 9.4T				Bovine Patellar Cartilage Specimens at 9.4T					
	Early OA		Advanced OA		CNT		GAG-		CA-	
	SZ	RZ	SZ	RZ	SZ	FZ	SZ	FZ	SZ	FZ
R_2^i(1/s)	11.5±0.5	19.5±2.2	6.1±0.2	16.4±1.2	8.7±0.2	12.9±0.5	6.5±0.2	10.4±0.8	2.7±0.1*	13.1±0.8
R_2^a(1/s)	26.4±0.7	68.0±3.2	8.0±0.3	33.2±1.4	9.9±0.6	22.1±2.0	12.3±1.1	17.7±1.5	1.64±0.1*	9.6±0.7
$\tau_b(\mu s)$	467±24	516±46	495±34	347±29	383±30	310±31	516±73	376±83	251±9	357±56
$S\ (10^{-3})$	1.89±0.05	2.88±0.15	1.01±0.04	2.46±0.11	1.28±0.05	2.12±0.12	1.23±0.09	1.72±0.20	0.64±0.01	1.30±0.11

*Standard deviations are less than 0.1 (1/s)

TABLE 3 The measured and modeled average $R_{1\rho}$ dispersion parameters in the femoral, tibial and patellar compartments from one healthy human knee in vivo at 3T. All data are reported as mean ± standard deviation.

	$R_{1\rho}$ (1/s) with $\omega_1/2\pi$ (kHz)					Fitted parameters			
	0.125	0.25	0.5	0.75	1.0	R_2^i(1/s)	R_2^a(1/s)	$\tau_b(\mu s)$	$S\ (10^{-3})$
femoral	19.2±5.4	18.2±4.1	15.2±3.2	14.1±2.7	13.9±3.2	11.7±2.9	11.3±4.9	272.7±146.3	1.74±0.53
tibial	19.4±3.4	19.7±2.5	17.5±2.8	15.8±2.0	15.0±1.5	12.7±1.7	8.7±4.1	198.8±152.8	1.82±0.64

patellar	16.7±4.0	18.7±3.7	12.4±1.6	12.2±1.9	11.4±1.9	9.4±2.1	10.8±4.1	171.7±49.1	1.97±0.33

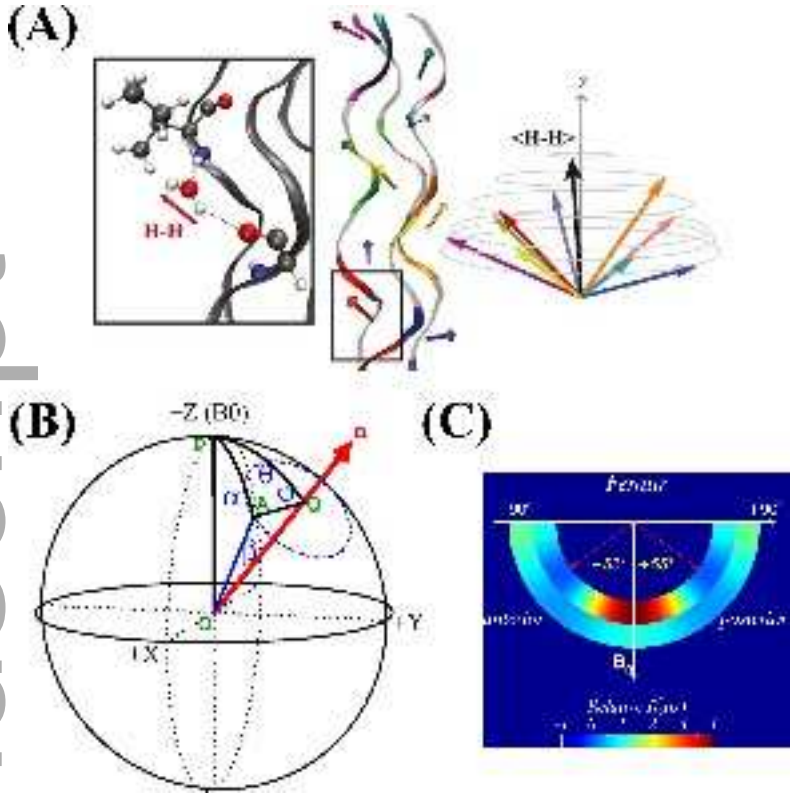

mrm_28045_f1.tif

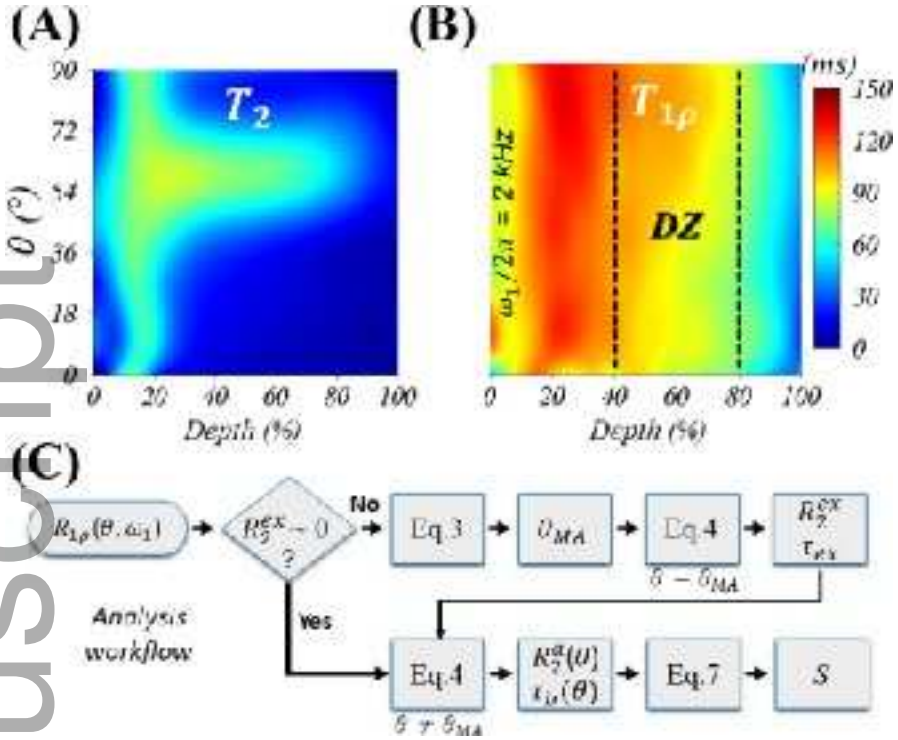

mrm_28045_f2.tif

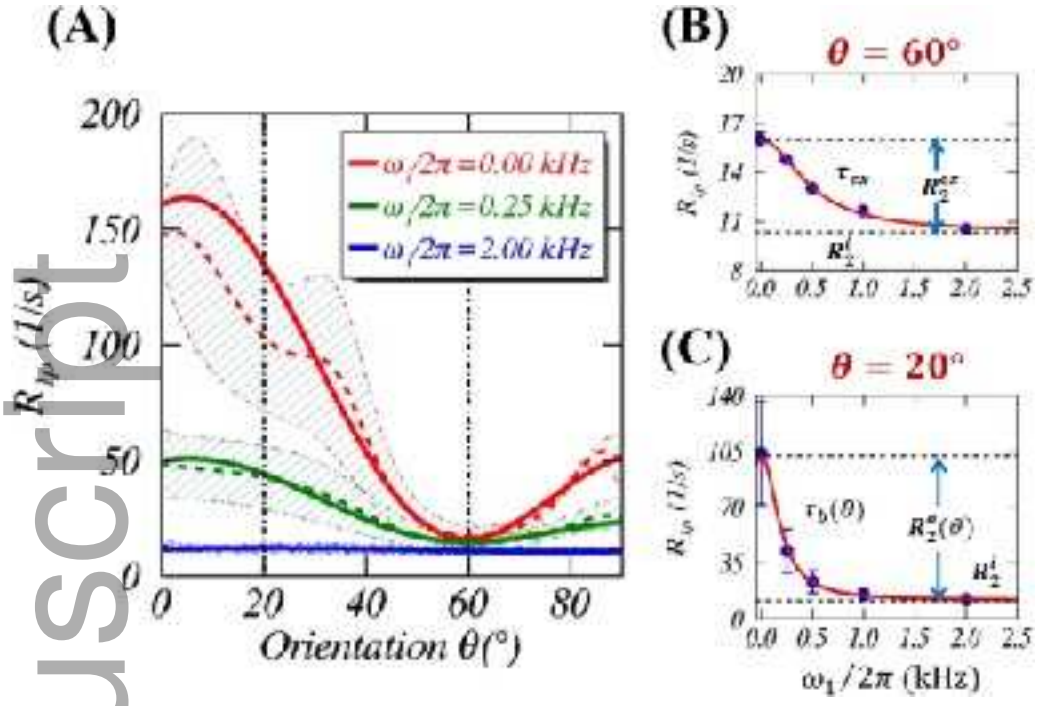

mrm_28045_f3.tif

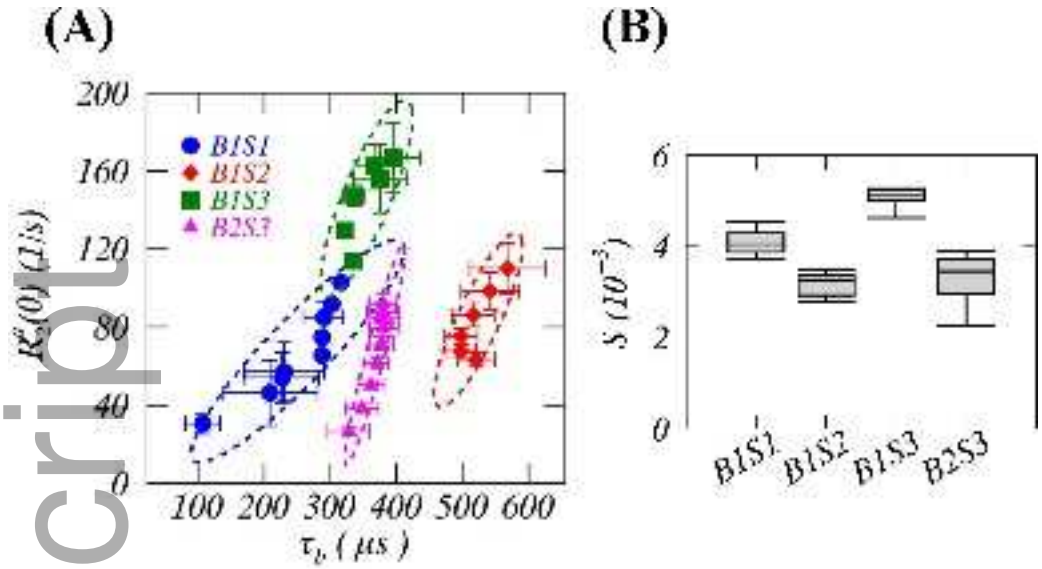

mrm_28045_f4.tif

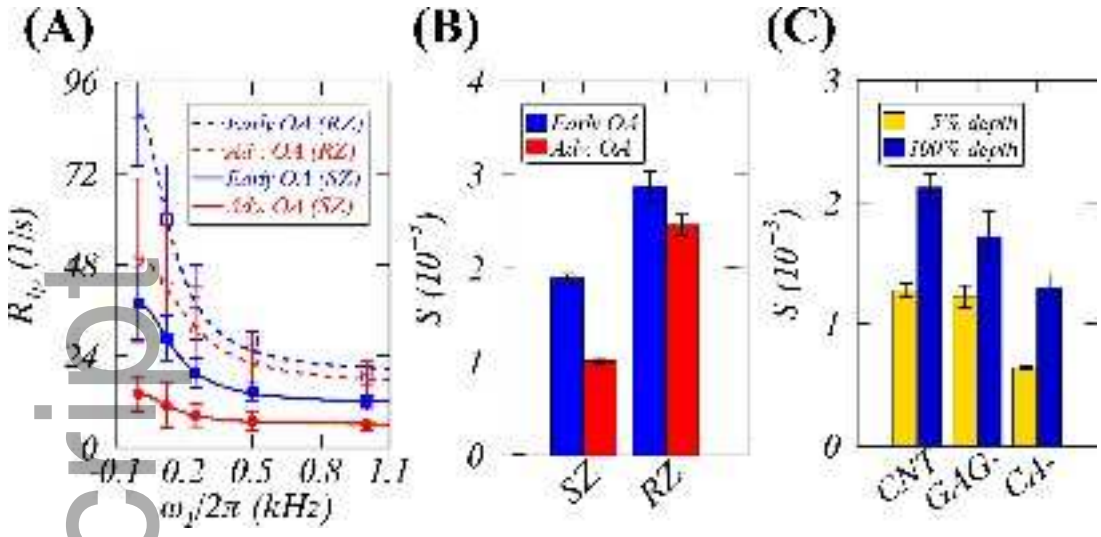

mrm_28045_f5.tif

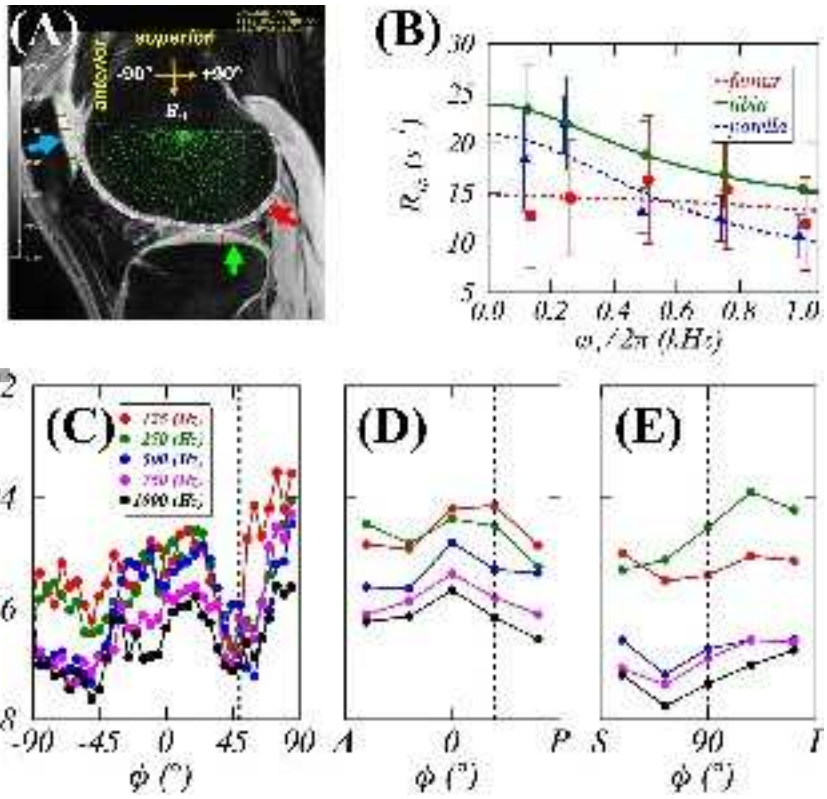

mrm_28045_f6.tif

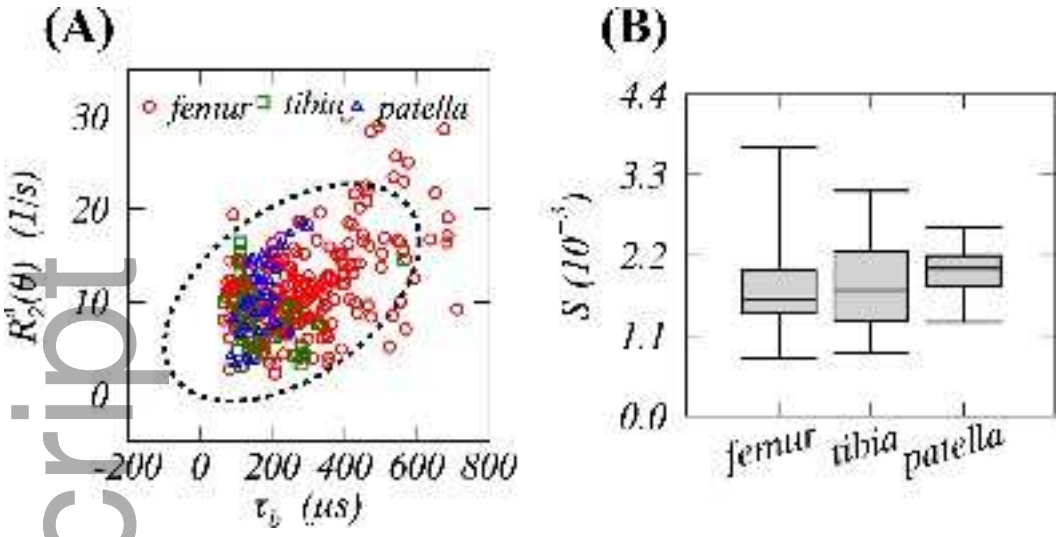

mrm_28045_f7.tif